

PULSAR WIND NEBULAE WITH THICK TOROIDAL STRUCTURE

Roger A. Chevalier¹ and Stephen P. Reynolds²

ABSTRACT

We investigate a class of pulsar wind nebulae that show synchrotron emission from a thick toroidal structure. The best studied such object is the small radio and X-ray nebula around the Vela pulsar, which can be interpreted as the result of interaction of a mildly supersonic inward flow with the recent pulsar wind. Such a flow near the center of a supernova remnant can be produced in a transient phase when the reverse shock reaches the center of the remnant. Other nebulae with a thick toroidal structure are G106.6+2.9 and G76.9+1.0. Their structure contrasts with young pulsar nebulae like the Crab Nebula and 3C 38, which show a more chaotic, filamentary structure in the synchrotron emission. In both situations, a torus-jet structure is present where the pulsar wind passes through a termination shock, indicating the flow is initially toroidal. We suggest that the difference is due to the Rayleigh-Taylor instability that operates when the outer boundary of the nebula is accelerating into freely expanding supernova ejecta. The instability gives rise to mixing in the Crab and related objects, but is not present in the nebulae with thick toroidal regions.

Subject headings: ISM: supernova remnants — pulsars: general

1. INTRODUCTION

The structure of a pulsar wind nebula is determined by the interaction of the relativistic pulsar wind with its surroundings, which are initially the parent supernova and later the interstellar medium. Pulsar nebulae are best observed by their synchrotron radio and X-ray emission, and three classes of nebulae can be characterized (Gaensler & Slane 2006). The first, typified by the Crab Nebula (Hester 2008), shows a small toroidal structure close to the

¹Department of Astronomy, University of Virginia, P.O. Box 400325, Charlottesville, VA 22904-4325; rac5x@virginia.edu

²Physics Department, North Carolina State University, Raleigh, NC 27695; reynolds@ncsu.edu

pulsar, and a more symmetric, larger scale structure. The outer boundary is formed where the shocked pulsar wind expands into the freely expanding gas of the parent supernova. The second, typified by Vela X, is formed after the reverse shock wave from the interaction with the interstellar medium moves back to the pulsar nebula (Blondin et al. 2001). This action displaces the pulsar nebula from the pulsar, leaving a ‘relic’ nebula. The third, typified by the Mouse (Gaensler et al. 2004), shows a trail of emission as the pulsar moves rapidly through the interstellar medium.

Here, we consider members of another class of pulsar nebula that is characterized by a thick toroidal emission region. In Section 2, we treat various members of this class, with special attention to the recently formed nebula surrounding the Vela pulsar. The distinguishing attributes of this class of pulsar nebula are discussed in Section 3.

2. PULSAR NEBULAE WITH THICK TOROIDAL EMISSION REGIONS

2.1. The Vela Nebula

The best studied example of a remnant with a likely asymmetric reverse shock is the Vela remnant, where a strong case can be made that a reverse shock from the N side of the remnant has displaced the original pulsar nebula (Vela X) from the pulsar (Blondin et al. 2001). While Vela X is now a relic nebula, the Vela pulsar has created a new nebula in its vicinity. Deep radio images of the region around the Vela pulsar show evidence for a bow wave (Figs. 9 and 10 of Dodson et al. 2003a, Fig. 1). The orientation of the bow wave is consistent with a flow from the N direction; the fact that the emission is strongest along a NE-SW line can be attributed to the orientation of the pulsar equatorial plane with this direction. Deep X-ray images show similar structure to that seen in the radio (Pavlov et al. 2003; Kargaltsev & Pavlov 2004). Pavlov et al. (2003) note that the X-ray jet to the NW tends to flop to the S, indicating the presence of a flow in that direction in the shocked pulsar wind.

The presence of a weak bow shock in Vela might seem surprising because the pulsar is centrally located in the larger remnant and van der Swaluw et al. (2004) showed that a moving pulsar must be at least 68% of the way to the outer shock in order to be moving supersonically. However, van der Swaluw et al. (2004) assume that the supernova remnant flow is described by the Sedov solution. There is a transition period before the Sedov solution is closely approximated. Considering a centrally located pulsar, the postshock region of the reverse shock (speed v_s) is characterized by a velocity $0.75v_s$ and sound speed $c_s = (5p/3\rho)^{1/2}$, with $p = 0.75\rho_0v_s^2$ and $\rho = 4\rho_0$ from the shock conditions, where ρ_0 is the preshock density.

The result is a Mach number $\mathcal{M} = v/c_s = 3/5^{1/2} = 1.3$ flow. If the pulsar has a velocity that carries it away from the center, it is comoving with the freely expanding gas, so that the properties of the postshock gas relative to the pulsar are the same as just described. If the reverse shock front has recently passed over the Vela pulsar, a mildly supersonic flow is naturally produced.

The observed radio emission marks the shocked pulsar wind and thus the black line in Fig. 1 delineates the contact discontinuity (CD) between the shocked pulsar wind and the shocked surrounding medium. The half-opening angle of the CD at large distances is $\sim 30^\circ$. The opening angle of the bow shock is expected to be larger (e.g., Fig. 8 of van der Swaluw et al. 2004). In flow past a blunt object, the half-opening angle, β , of the shock wave that is generated obeys $\sin \beta = c_s/v = 1/\mathcal{M}$, where c_s is the gas sound speed, v is the gas velocity, and \mathcal{M} is the Mach number (e.g., Landau & Lifshitz 1959). The expected $\mathcal{M} = 1.3$ flow thus gives a half-opening angle for the bow shock of 50° , which is roughly consistent with the observations. The implication is that there is a mildly supersonic flow past the pulsar nebula.

The direction of pulsar motion is known (position angle 301° , Dodson et al. 2003b) and does not line up with the displacement of Vela X or the bow shock discussed here. The flow velocity involved in the displacement of Vela X is $v_d = 500(r_d/5 \text{ pc})(t_d/2500 \text{ yr})^{-1} \text{ km s}^{-1}$, where r_d is the displacement distance estimated for the center of the relic pulsar nebula and t_d is the age since the displacement began. The temperature in the central region of Vela is $\sim 1.2 \text{ keV}$ (Lu & Aschenbach 2000), yielding a sound speed of 560 km s^{-1} , although there are also cooler components. The flow velocities associated with the reverse shock are apparently much larger than the projected velocity of the Vela pulsar, 61 km s^{-1} (Dodson et al. 2003b), so that the pulsar velocity does not play a significant role in the orientation of the flow past the pulsar, in agreement with observations. If the surroundings of the pulsar have been cleared so that the pulsar interacts directly with the thermal gas, a mildly supersonic flow past the pulsar is expected.

Some properties of the Vela pulsar nebula are given in Table 1. The nebular pressure P_n at the termination shock (assumed to be the torus radius R_{torus}) is given by pressure balance $P_n = \dot{E}/(4\pi R_{\text{torus}}^2 c) = 2 \times 10^{-9} \text{ dyn cm}^{-2}$ for the parameters in Table 1, where \dot{E} is the spindown power of the pulsar. If half of this pressure is supplied by the magnetic field, we have $B = 1.6 \times 10^{-4} \text{ G}$. Assuming $\gamma = 4/3$ for the shocked pulsar wind and a uniform pressure, the energy (within the nebular radius R_{radio}) is $E_{\text{neb}} = 3.6 \times 10^{45} \text{ ergs}$. The minimum energy, E_{min} , required to produce the synchrotron emission from the Vela nebula can be estimated. The total flux of the radio nebula is 1 Jy and has a flat spectrum between 1.4 and 8.5 GHz (Dodson et al. 2003a). Extrapolating the low energy X-ray emission, with

$\alpha = -0.66$ where $F_\nu \propto \nu^\alpha$ (Mangano et al. 2005), yields a break frequency of 3×10^{10} Hz. Equation (46) of Chevalier (2005) for the minimum energy then yields $E_{min} = 4 \times 10^{44}$ ergs. The energy estimated above is $E_{neb} \sim 10$ times the minimum. The time for the pulsar spindown to produce this energy is $E_{neb}/\dot{E} = 17$ yr. Radiative losses are small and adiabatic expansion losses are not expected to change this estimate by a large factor ($\lesssim 2$), so the age of the particles in the radio nebula is relatively small. Older particles are swept downstream in the SE direction, as can be seen in deep radio and X-ray images (Dodson et al. 2003a; Kargaltsev & Pavlov 2004).

As mentioned above, the spectrum of the total radio flux is flat, or slowly declining, which is typical of pulsar wind nebulae. However, Dodson et al. (2003a) find large (several 0.1's) variation in α over the nebula when examined over the separate frequency ranges. Also surprising is that in some places $\alpha > 1/3$, which is not expected for optically thin synchrotron radiation. Bietenholz et al. (1991) measured $\alpha = -0.6$ between 1.4 and 5 GHz for the bright part of the radio nebula to the NE, which also indicates variations in spectral index. This situation contrasts with that of the Crab and related nebulae, where spatial variations in radio spectral index are small. For the Crab, Bietenholz et al. (1997) find that the α is constant to an accuracy of 0.01. Although the limit on variation is weaker in the case of 3C 58, the spectral index is also fairly constant (Bietenholz et al. 2001). These properties suggest that there are mixing or diffusive processes going on in the Crab and 3C 58 that are not present in the Vela nebula.

The morphology of the Vela radio nebula contrasts with the pre-reverse shock pulsar nebulae. The magnetic field is predominantly toroidal, with the linear polarization reaching 60% (Dodson et al. 2003a). Filamentary structure with a scale comparable to the termination shock radius, as seen in younger nebulae, is not apparent. The radio nebula is smaller than in the pre-reverse shock cases, but $R_{radio}/R_{torus} = 5 - 6$; the angular size of the structures is comparable to the case of the Crab Nebula. We suggest that the absence of structure is due to a combination of the facts that the outer boundary is not subject to the Rayleigh-Taylor instability in this case and that only relatively recent effects of the pulsar wind are observed. The strong emission in the pulsar equatorial plane can be attributed to the stronger pulsar power in this direction, as expected in a split monopole model for the pulsar wind (Bogovalov 1999). The dynamics of the nebula depend on a complex 3-dimensional situation because the rotation axis is not aligned with the direction of the surrounding flow. The fact that a jet-torus structure is present around the pulsar suggests that the magnetization parameter $\sigma \approx 0.1$ in the pulsar wind (Bucciantini 2011) and that the magnetic field reaches equipartition strength in the downstream flow. Once the magnetic field reaches this strength in a bow shock situation, it tends to increase the size of the wind nebula between the termination shock and the contact discontinuity (Bucciantini et al. 2005a), so the contact discontinuity

is at several times the termination shock radius, as observed in the Vela nebula.

Another indication of significant magnetic forces in the nebula is the central position of the pulsar in the inner X-ray nebula (Fig. 1, Ng & Romani 2004). In a hydrodynamic model in which the pressure is constant between the contact discontinuity and the pulsar wind termination shock, the ratio of the termination shock radius on the upstream side to that on the downstream side is $1/\mathcal{M}$ (van der Swaluw et al. 2003). Assuming that the inner X-ray nebula represents the termination shock and $\mathcal{M} \approx 1.3$, the displacement expected in the hydrodynamic model is not present. However, significant pressure forces from a toroidal magnetic field give a decreasing pressure with radius and the pressure gradient can be larger than the pressure differential from the bow shock estimated here (Kennel & Coroniti 1984; Emmering & Chevalier 1987).

We have examined simple models for the projected radio emission in which there is uniform emission from a toroidal region with an inner and outer radius, and an opening angle. Fig. 2 shows a model that resembles the radio structure (Dodson et al. 2003a): the outer radius is 5 times the inner radius, which is assumed to be at the position of the inner X-ray torus, the half-angle of the disk is 35° , and the angle between the line of sight and the axis of the torus is $\zeta = 50^\circ$. The emissivity is assumed to be uniform and isotropic, which would be appropriate for a region with a tangled magnetic field. However, the observed radio polarization at 5 GHz (Dodson et al. 2003a) is the maximum expected for a flat flux spectrum, suggesting that the magnetic field is ordered. Emission in a purely toroidal field would enhance the emission along the minor axis compared to the major axis and thus reduce the agreement with the observed morphology. Models for the synchrotron emission from the central region of the Crab based on relativistic MHD simulations show reasonable agreement with the observations (Bucciantini et al. 2005b; Del Zanna et al. 2006). The outer parts of ring-like structures are enhanced when the magnetic field is taken to be isotropic as opposed to toroidal (Del Zanna et al. 2006, their Figs. 3 and 4). Del Zanna et al. (2006) also find the effects of the mildly relativistic flow are significant. In our case, the radial velocity drops beyond the termination shock so that relativistic effects are not important.

The observed emission from the Vela nebula shows a high surface brightness to the NE (Dodson et al. 2003a), presumably due to the low Mach number flow. The flow is probably also responsible for the higher surface brightness to the NW along the minor axis, and possibly for the brighter X-ray “outer jet” to the NW even though its motion is expected to be directed away from us based on the brightness distributions of the inner tori (Pavlov et al. 2003; Ng & Romani 2004). The angle ζ in our model is somewhat less than that found by Ng & Romani (2004) for the inner toroidal X-ray structure around the pulsar ($\zeta = 63.6^\circ$); again, the difference may be related to the bow shock flow. Three-dimensional MHD simu-

lations will ultimately be needed to model the emission.

The X-ray emission is observed to extend out to the same place as the radio (Kargaltsev & Pavlov 2004). The age of the nebula and the magnetic field strength indicate a synchrotron cooling break in the X-ray range and Mangano et al. (2005) find an apparent cooling break in the spectrum at 12.5 keV. This would explain the similar extent at radio and X-ray wavelengths.

2.2. G106.6+2.9

Another nebula with similar properties to the Vela nebula is G106.6+2.9 (also known as the Boomerang), associated with J2229+6114 (Table 1). Unfortunately, the distance is poorly known, with estimates of 800 pc based on low radio depolarization and interaction with neutral gas (Kothés et al. 2001), 3 kpc based on X-ray absorption (Halpern et al. 2001), and 7.5 kpc based on pulsar dispersion measure (Abdo et al. 2009). We scale the distance, d , with $d_3 = d/(3 \text{ kpc})$. The Boomerang has considerable radio emission on one side and Kothés et al. (2006) identified this structure as the result of an asymmetric reverse shock, although a larger scale thermal remnant is not observed around the nebula. In this case, the pulsar \dot{E} and R_{torus} suggest $P_n = 3.3 \times 10^{-10} d_3^{-2} \text{ dyn cm}^{-2}$. The magnetic field and the radio nebula energy, computed as for Vela, are $B = 6.5 \times 10^{-5} d_3^{-1} \text{ G}$ and $E_{\text{neb}} = 2.7 \times 10^{47} d_3 \text{ ergs}$. The minimum energy in the radio nebula is $2.4 \times 10^{46} d_3^{17/7} \text{ ergs}$. The time for the pulsar to produce the nebular energy is again relatively short, $\sim 390 d_3 \text{ yr}$.

The radio nebula is highly polarized, up to 50%, indicating a toroidal field component (Kothés et al. 2006). The radio spectrum shows $\alpha = -0.11 \pm 0.05$ below 4.3 GHz and $\alpha = -0.59 \pm 0.09$ above, which Kothés et al. (2006) interpret as a synchrotron cooling break; they note that there is a steeper spectrum farther from the pulsar. To obtain such a low cooling break frequency, Kothés et al. (2006) need a magnetic field of 2.6 mG and particle lifetime of 3900 yr in a model with $d_3 = 0.27$. We find that this field would produce too high a pressure in the nebula and the age is longer than expected, so that the spectral break is likely to be intrinsic to the injection.

Kothés et al. (2006) propose that the variations in rotation measure across the remnant are intrinsic to the remnant because of the apparent symmetry about an axis defined by the polarized emission. For the magnetic field we have derived, an electron density $n_e \gtrsim 1/f \text{ cm}^{-3}$, where f is the filling factor would be needed in the remnant to produce the rotation measure. In our view, n_e is much lower than this value because the pulsar wind bubble has smoothly expanded into the surrounding medium, so the apparent alignment of the rotation measure pattern is a coincidence.

2.3. G76.9+1.0

The remnant G76.9+1.0 has a similar radio morphology to the Vela nebula, and *Chandra* observations show that the radio lobes have a similar orientation compared to the axis of the pulsar rotation (Arzoumanian et al. 2011). However, it differs from the Vela nebula in 2 important ways: it is much larger (29×35 pc at a distance of 10 kpc) and the large scale nebula has symmetry about the pulsar. These properties indicate that the pulsar nebula has not been affected by the reverse shock wave. We suggest that the inward mixing of thermal filaments has not been so efficient in this case so that a toroidal emission region has a chance to build up, as in the case of the Vela nebula. The instabilities are expected to be strongest during the constant \dot{E} phase of the pulsar evolution. Once a pulsar is no longer adding substantially to the energy of the remnant, the acceleration ceases. This might be expected in a large pulsar nebula where a low density surroundings has delayed the action of the reverse shock wave.

3. DISCUSSION

Pulsars are expected to preferentially inject their wind power close to the equatorial plane and models that allow for such power injection (Komissarov & Lyubarsky 2003; Del Zanna et al. 2004) have been successful in reproducing many of the properties of the torii observed immediately surrounding the pulsars in young wind nebulae. However, on a larger scale (several inner torus radii), the young nebulae such as the Crab and 3C 58 do not show the toroidal structure. Here we have investigated the evolutionary status of several pulsar nebulae, best exemplified by the newly formed Vela nebula, that do show a thick toroidal structure. We suggest that the structure is not present in the Crab and related objects because of Rayleigh-Taylor instabilities at the interface between the expanding supernova gas and the accelerating pulsar nebula (Chevalier 1977; Hester 2008), although there remain uncertainties in the instability when the light fluid is magnetized (Bucciantini et al. 2004; Stone & Gardiner 2007). The instabilities give rise to mixing and diffusion of the relativistic particles. In the cases discussed here, the instability is absent either because the outer boundary is determined by a somewhat asymmetric outer pressure or the pulsar power has declined so the outer boundary is no longer accelerated. The age at this phase is $\sim 10^4$ yr, within a factor of a few. In the case of an asymmetric outer pressure, a relic pulsar nebula may also be present, as in the case of the Vela nebula. At later times, the pulsar velocity leads to a nebular trail to the pulsar.

Multidimensional simulations are needed to confirm the scenario proposed here. In their numerical simulations of pulsar nebulae, Camus et al. (2009) find that waves and vortices in

the larger nebula feed back on the structure at the termination shock, which in turn generates more structure in the nebula; they note that it is impossible to distinguish between the cause and the effect. In addition, some thermal gas from the supernova is entrained in the unstable region, explaining the optical filaments seen in association with nonthermal filaments in the Crab and 3C 58. These were 2-dimensional simulations, but did not impose symmetry about the equatorial plane. More investigation of the instabilities and 3-dimensional simulations are ultimately needed (e.g., Mizuno et al. 2011).

We are grateful to Richard Dodson for permission to use the image shown in Fig. 1, and to the referee for helpful comments. This research was supported in part by NASA grant NNX07AG78G.

REFERENCES

- Abdo, A. A., et al. 2009, *ApJ*, 706, 1331
- Arzoumanian, Z., Gotthelf, E. V., Ransom, S. M., Safi-Harb, S., Kothes, R., & Landecker, T. L. 2011, *ApJ*, submitted (arXiv:1105.3185)
- Bietenholz, M. F., Frail, D. A., & Hankins, T. H. 1991, *ApJ*, 376, L41
- Bietenholz, M. F., Kassim, N., Frail, D. A., Perley, R. A., Erickson, W. C., & Hajian, A. R. 1997, *ApJ*, 490, 291
- Bietenholz, M. F., Kassim, N. E., & Weiler, K. W. 2001, *ApJ*, 560, 772
- Blondin, J. M., Chevalier, R. A., & Frierson, D. M. 2001, *ApJ*, 563, 806
- Bogovalov, S. V. 1999, *A&A*, 349, 1017
- Bucciantini, N. 2011, in *High-Energy Emission from Pulsars and their Systems*, ed. N. Rea & D. Torres (Berlin: Springer), 473 (arXiv:1005.4781)
- Bucciantini, N., Amato, E., Bandiera, R., Blondin, J. M., & Del Zanna, L. 2004, *A&A*, 423, 253
- Bucciantini, N., Amato, E., & Del Zanna, L. 2005a, *A&A*, 434, 189
- Bucciantini, N., del Zanna, L., Amato, E., & Volpi, D. 2005b, *A&A*, 443, 519
- Camus, N. F., Komissarov, S. S., Bucciantini, N., & Hughes, P. A. 2009, *MNRAS*, 400, 1241

- Chevalier, R. A. 1977, in *Supernovae*, ed. D. N. Schramm (Dordrecht: Reidel), 53
- Chevalier, R. A. 2005, *ApJ*, 619, 839
- Del Zanna, L., Amato, E., & Bucciantini, N. 2004, *A&A*, 421, 1063
- Del Zanna, L., Volpi, D., Amato, E., & Bucciantini, N. 2006, *A&A*, 453, 621
- Dodson, R., Lewis, D., McConnell, D., & Deshpande, A. A. 2003a, *MNRAS*, 343, 116
- Dodson, R., Legge, D., Reynolds, J. E., & McCulloch, P. M. 2003b, *ApJ*, 596, 1137
- Emmering, R. T., & Chevalier, R. A. 1987, *ApJ*, 321, 334
- Gaensler, B. M., & Slane, P. O. 2006, *ARA&A*, 44, 17
- Gaensler, B. M., van der Swaluw, E., Camilo, F., Kaspi, V. M., Baganoff, F. K., Yusef-Zadeh, F., & Manchester, R. N. 2004, *ApJ*, 616, 383
- Halpern, J. P., Gotthelf, E. V., Leighly, K. M., & Helfand, D. J. 2001, *ApJ*, 547, 323
- Hester, J. J. 2008, *ARA&A*, 46, 127
- Kargaltsev, O., & Pavlov, G. 2004, in *Young Neutron Stars and Their Environments*, IAUS 218, ed. F. Camilo & B. M. Gaensler (San Francisco: ASP), 195
- Kennel, C. F., & Coroniti, F. V. 1984, *ApJ*, 283, 694
- Komissarov, S. S., & Lyubarsky, Y. E. 2003, *MNRAS*, 344, L93
- Kothes, R., Uyaniker, B., & Pineault, S. 2001, *ApJ*, 560, 236
- Kothes, R., Reich, W., & Uyaniker, B. 2006, *ApJ*, 638, 225
- Landau, L. D., & Lifshitz, E. M. 1959, *Fluid Mechanics* (London: Pergamon)
- Lu, F. J., & Aschenbach, B. 2000, *A&A*, 362, 1083
- Mangano, V., Massaro, E., Bocchino, F., Mineo, T., & Cusumano, G. 2005, *A&A*, 436, 917
- Mizuno, Y., Lyubarsky, Y., Nishikawa, K.-I., & Hardee, P. E. 2011 *ApJ*, 728, 90
- Ng, C.-Y., & Romani, R. W. 2004, *ApJ*, 601, 479
- Pavlov, G. G., Teter, M. A., Kargaltsev, O., & Sanwal, D. 2003, *ApJ*, 591, 1157
- Stone, J. M., & Gardiner, T. 2007, *ApJ*, 671, 1726

van der Swaluw, E., Achterberg, A., Gallant, Y. A., Downes, T. P., & Keppens, R. 2003, A&A, 397, 913

van der Swaluw, E., Downes, T. P., & Keegan, R. 2004, A&A, 420, 937

Table 1. Properties of Pulsars and their Nebulae

PSR	Supernova Remnant	Distance (kpc)	\dot{E}/I_{45} (ergs s ⁻¹)	τ_{char} (yr)	R_{torus} (pc)	R_{radio} (pc)	Refs.
B0833–45	Vela	0.29	6.9×10^{36}	1.1×10^4	0.030	0.17	1,2,3
J2229+6114	G106.6+2.9	$3d_3$	2.2×10^{37}	1.05×10^4	$0.13d_3$	$1.3d_3$	4,3

References.– (1) Dodson et al. (2003b); (2) Dodson et al. (2003a); (3) Ng & Romani (2004); (4) Kothes et al. (2006)

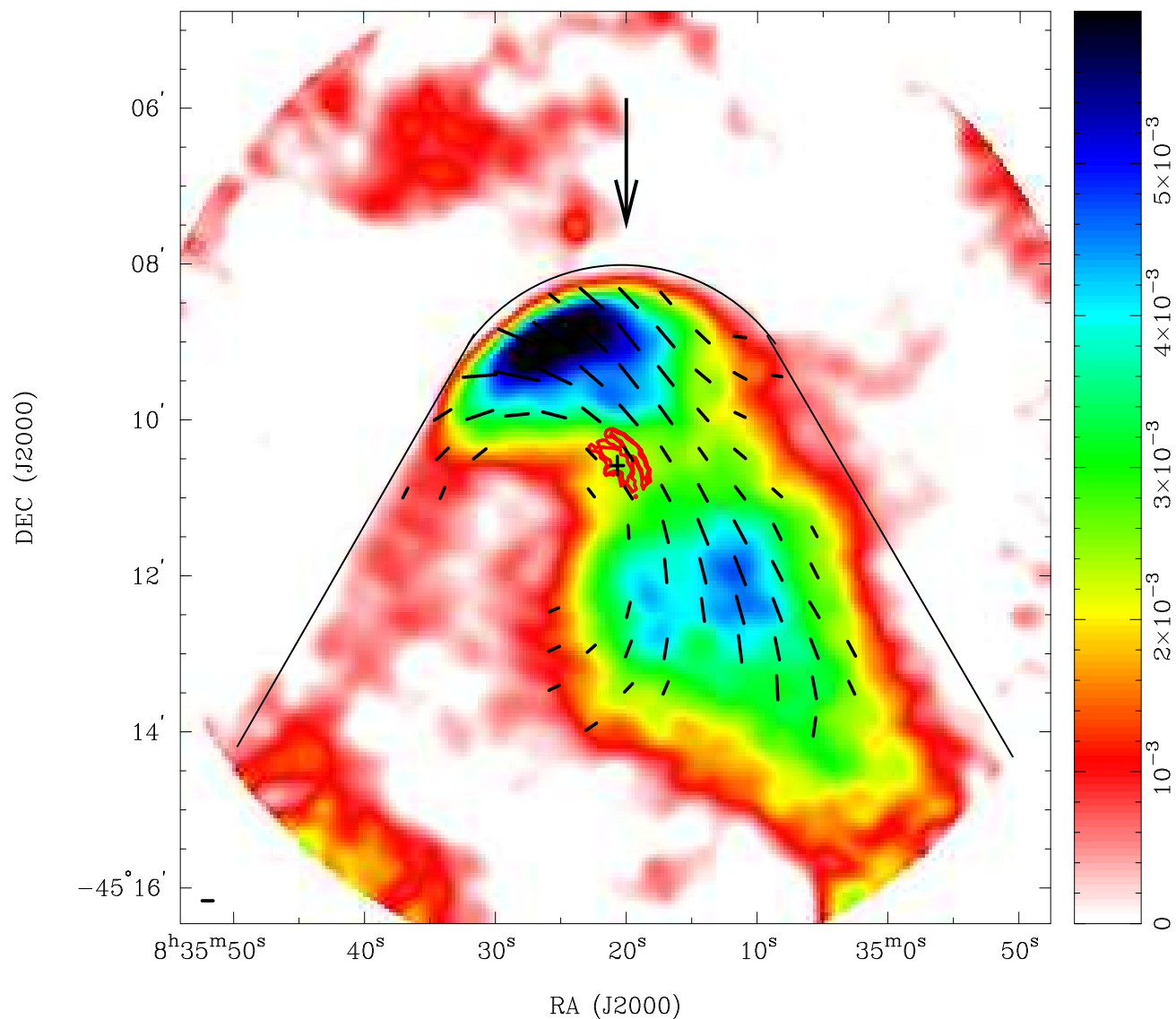


Fig. 1.— The image, reproduced from Fig. 10 of Dodson et al. (2003a), shows the Vela nebula at 5 GHz, with derotated magnetic field lines and Chandra X-ray contours overlaid. The cross marks the pulsar position. The solid black line is the suggested contact discontinuity between the shocked pulsar wind and gas that has passed through the bow shock. The arrow indicates the direction of the mildly supersonic flow.

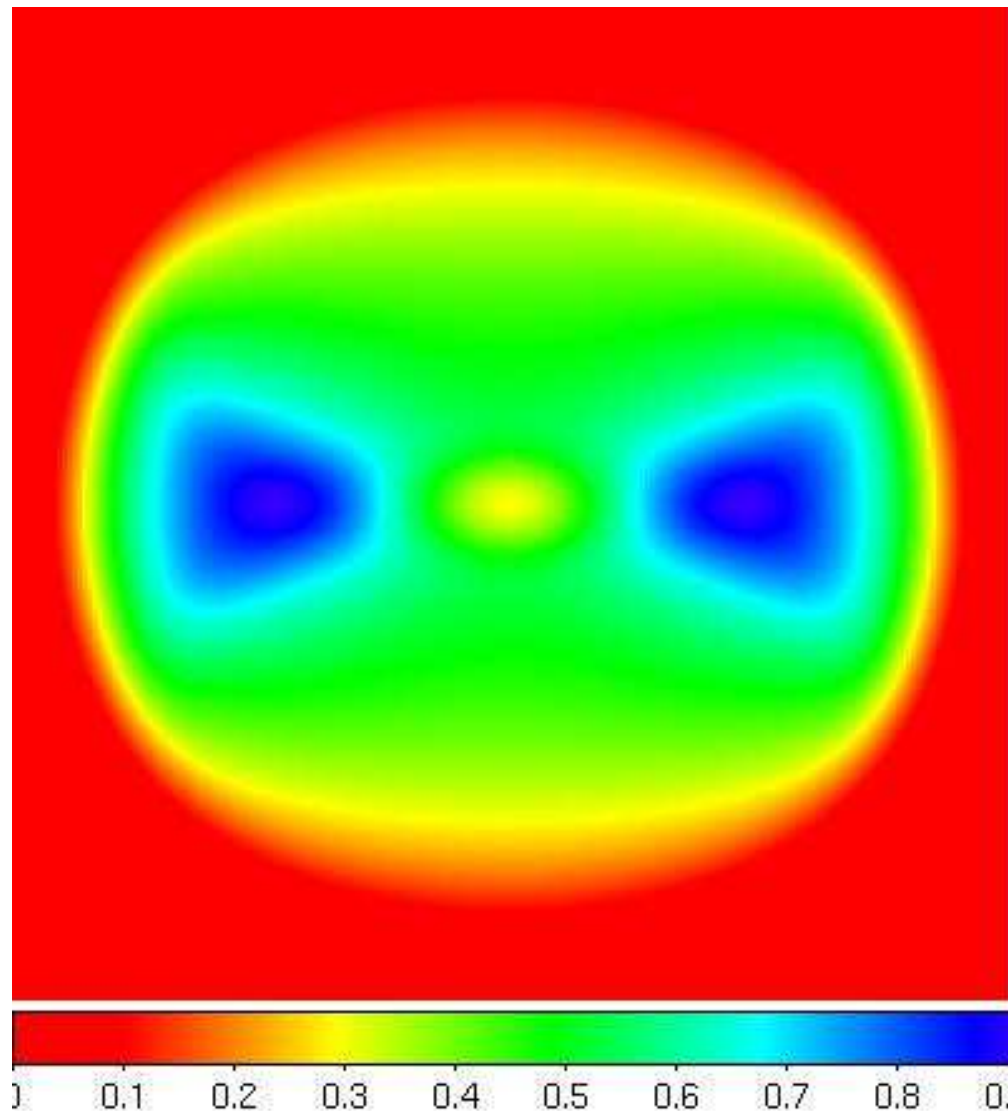


Fig. 2.— Model of a toroidal region with uniform emissivity seen in projection with the axis tilted 50° to the line of sight. The disk half-angle is 35° and the maximum radius is 5 times the inner radius. The color scale is linear.